Electronic Supplementary Material (ESI) for ChemComm.

Supporting Information

Competition of cation-π and exo-wall π-π interactions, a novel approach to achieve ultrasensitive response

You-Ming Zhang,* Wei Zhu, Wen-Juan Qu, Kai-Peng Zhong, Xiao-Peng Chen, Hong Yao, Tai-Bao Wei, and Qi Lin*

Key Laboratory of Eco-Environment-Related Polymer Materials, Ministry of Education of China, Key Laboratory of Polymer Materials of Gansu Province, College of Chemistry and Chemical Engineering, Northwest Normal University, Lanzhou, Gansu, 730070, P. R. China

Contents

Materials and methods

Scheme S1 Synthesis of compound [**1**-**3**] and **P5N**.

Fig. S1 ^{1}H NMR spectrum of compound **1** in $CDCl_3$.

Fig. S2 ^{13}C NMR spectrum of compound **1** in $CDCl_3$.

Fig. S3 ESI-MS spectrum of compound **1**.

Fig. S4 ^{1}H NMR spectrum of compound **2** in $CDCl_3$.

Fig. S5 ^{13}C NMR spectrum of compound **2** in $CDCl_3$.

Fig. S6. ESI-MS spectrum of compound **2**.

Fig. S7 ^{1}H NMR spectrum of compound **3** in DMSO-d_6.

Fig. S8 ^{13}C NMR spectrum of compound **3** in DMSO-d_6.

Fig. S9 ESI-MS spectrum of compound **3**.

Fig. S10 ^{1}H NMR spectrum of **P5N** in DMSO-d_6.

Fig. S11 ^{13}C NMR spectrum of **P5N** in $CDCl_3$.

Fig. S12 ESI-MS spectrum of **P5N**.

Scheme S2 Synthesis of compound [**4**-**5**].

Fig. S13 ^{1}H NMR spectrum of compound **4** in $CDCl_3$.

Fig. S14 ^{13}C NMR spectrum of compound **4** in $CDCl_3$.

Fig. S15 ESI-MS spectrum of compound **4**.

Fig. S16 ^{1}H NMR spectrum of compound **5** in $CDCl_3$.

Fig. S17 ^{13}C NMR spectrum of compound **5** in $CDCl_3$.

Fig. S18 ESI-MS spectrum of compound **5**.

Calculation method of emission quantum yield

Table S1. Gelation Properties of Organogel **P5N-OG** in Organic Solvents

Fig. S19 Temperature-dependent fluorescence spectra of **P5N-OG** (in cyclohexanol, 5% (w/v)) during gelation process (λ_{ex} = 297 nm).

Fig. S20 Partial concentrations-dependent ^{1}HNMR spectra of **P5N** in $CDCl_3$, from bottom to top: 3.7 × 10^{-3} M, 9.3 × 10^{-3} M, 1.9 × 10^{-2} M, 2.8 × 10^{-2} M, 3.7 × 10^{-2} M.

Fig. S21 2D NOESY NMR spectrum of **P5N** (30 mM) in DMSO-d_6 solution.

Fig. S22 2D NOESY NMR spectrum of **P5N** (30 mM) in $CDCl_3$ solution.

Fig. S23 FT-IR spectra of powdered **P5N**, xerogel **P5N-OG**, xerogel **P5N-FeG**, and xerogel **P5N-FeG** + $H_2PO_4^-$.

Fig. S24 Powder XRD patterns of xerogel **P5N-OG**, xerogel **P5N-FeG**, and xerogel **P5N-FeG** + $H_2PO_4^-$.

Fig. S25 Fluorescence spectra of permethyl-pillar[5]arene (compound **4**) in the presence of different concentration of naphthalimide monomer (compound **5**) in cyclohexanol at room temperature (λ_{ex} = 265 nm).

Fig. S26 Job's plot showing the 2:1 stoichiometry of the complexation between permethyl-pillar[5]arene (model compound **4**) (2×10^{-4} M) and naphthalimide monomer (model compound **5**) (0.1 M) in cyclohexanol by plotting the fluorescence intensity at λ_{ex} = 265 nm.

Fig. S27 SEM images of (a) powder **P5N**; (b) xerogel **P5N-OG**; (c) xerogel **P5N-FeG**; (c) xerogel **P5N-FeG** + $H_2PO_4^-$.

Fig. S28 Fluorescence spectra of **P5N-OG** (in cyclohexanol, 5% (w/v)) with increasing concentration of Fe^{3+} (λ_{ex} = 297 nm).

Fig. S29 A plot of emission at 530 nm versus number of equivalents of Fe^{3+}.

Fig. S30 The photograph of the linear range for Fe^{3+}.

Table S2. Comparison of the Analytical Performance of the Fluorescence Sensing Systems for Fe^{3+}.

Fig. S31 Fluorescence spectra of **P5N-OG** (in cyclohexanol, 5% (w/v)) in the presence of solid samples of iron (III) perchlorate hexahydrate (0.00094 g, 0.29 equiv.) at room temperature (λ_{ex} = 297 nm).

Fig. S32 Fluorescence spectra of **P5N-OG** (in cyclohexanol, 5% (w/v)) in the presence of various anions (F^-, Cl^-, Br^-, I^-, AcO^-, $H_2PO_4^-$, HSO_4^-, ClO_4^-, SCN^-, and CN^-) at room temperature (λ_{ex} = 297 nm).

Fig. S33 Fluorescence spectra of **P5N-FeG** (in cyclohexanol, 5% (w/v)) with increasing concentration of $H_2PO_4^-$ (λ_{ex} = 297 nm).

Fig. S34 A plot of emission at 530 nm versus number of equivalents of $H_2PO_4^-$.

Fig. S35 The photograph of the linear range for $H_2PO_4^-$.

Fig. S36 Fluorescent "on-off-on" cycles of **P5N-OG**, controlled by the alternative addition of Fe^{3+} and $H_2PO_4^-$ (λ_{ex} = 297 nm).

Table S3. The ICP Date of **P5N-OG** with Fe^{3+}.

Fig. S37 Recyclable separation of Fe^{3+} (λ_{ex} = 297 nm).

Fig. S38 Fluorescence spectra of **P5N-OG** (in cyclohexanol, 5% (w/v)) in different concentration of Fe^{3+} at room temperature (λ_{ex} = 297 nm).

Table S4. The ICP Date of Tap Water with Fe^{3+}.

Materials and methods

Fresh double distilled water was used throughout the experiment. All other reagents and solvents were commercially available at analytical grade and were used without further purification. All anions and cations were purchased from Alfa Aesar and used as received. ^{1}H NMR spectra were recorded on a Mercury-600 BB spectrometer at 600 MHz and a Mercury-400 BB spectrometer at 400 MHz, ^{13}C NMR spectra were recorded on a Mercury-600 BB spectrometer at 151 MHz and a Mercury-400 BB spectrometer at 101 MHz. Chemical shifts are reported in ppm downfield from tetramethylsilane (TMS, δ scale with the solvent resonances as internal standards). Photoluminescence spectra were performed on a Shimadzu RF-5301PC fluorescence spectrophotometer. Mass spectra were performed on a Bruker Esquire 3000 plus mass spectrometer (Bruker-Franzen Analytik GmbH Bremen, Germany) equipped with ESI interface and ion trap analyzer. Melting points were measured on an X-4 digital melting-point apparatus and were uncorrected. The infrared spectra were performed on a Digilab FTS-3000 FTIR spectrophotometer. The X-ray diffraction analysis (XRD) was performed in a transmission mode with a Rigaku RINT2000 diffractometer equipped with graphite monochromated CuKa radiation (λ = 1.54073 Å). The morphologies and sizes of xerogels were characterized using field emission scanning electron microscopy (FE-SEM, JSM-6701F) at an accelerating voltage of 8 kV.

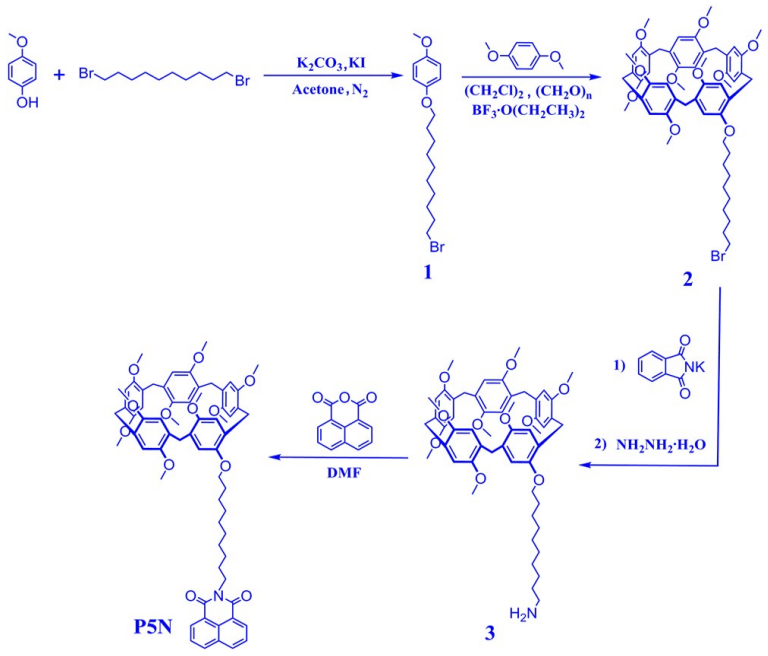

Scheme S1 Synthesis of compound [**1-3**] and **P5N**.

Synthesis of compound 1. A mixture of 4-methoxyphenol (2.48 g, 20.0 mmol), K_2CO_3 (13.82 g, 100 mmol), KI (3.32 g, 20 mmol), 1,10-dibormodecane (24.01 g, 80 mmol) and acetone (400.0 mL) were added to a 500 mL round-bottom flask under nitrogen atmosphere. The reaction mixture was stirred at 65 ℃ for 72 h. After the solid was filtered off, the solvent was

evaporated and the residue was dissolve in CH_2Cl_2. The crude product was purified by silica gel column chromatography using petroleum ether/ethyl acetate (V/V = 50:1) as the eluent, compound **1** as white solid (6.53 g, yield 95%) was isolated. Mp: 60-62 ℃. ^{1}H NMR ($CDCl_3$, 600 MHz), δ/ppm: 6.83 (s, 4H), 3.91-3.89 (t, *J* = 6.6 Hz, 2H), 3.76 (s, 3H), 3.41-3.39 (t, *J* = 6.9 Hz, 2H), 1.86-1.82 (m, 2H), 1.77-1.72 (m, 2H), 1.45-1.41 (m, 2H), 1.35-1.30 (m, 10H). ^{13}C NMR ($CDCl_3$, 151 MHz), δ/ppm: 153.64, 153.27, 115.41, 114.59, 68.62, 55.73, 34.01, 32.81, 30.47, 29.42, 29.36, 29.33, 28.72, 28.14, 26.02. ESI-MS m/z: calcd for $C_{17}H_{27}BrO_2$ [**1**]: 342.12; found: 342.01.

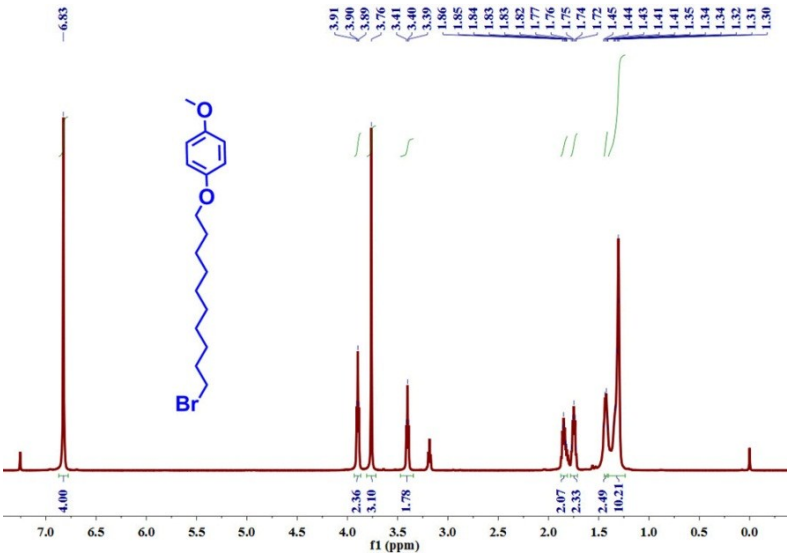

Fig. S1 ^{1}H NMR spectrum of compound **1** in $CDCl_3$.

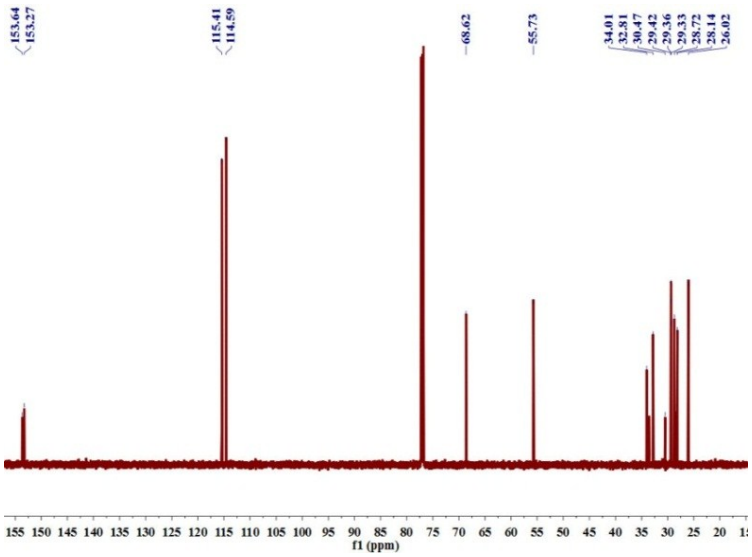

Fig. S2 ^{13}C NMR spectrum of compound **1** in $CDCl_3$.

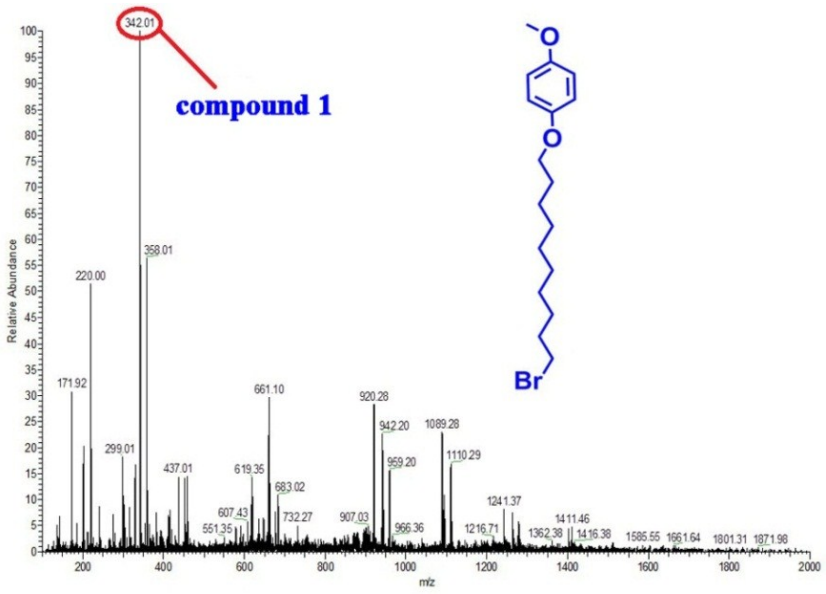

Fig. S3 ESI-MS spectrum of compound **1**.

Synthesis of compound 2. 1-(10-bromodecyloxy)-4-methoxybenzene (compound **1**) (1.72 g, 5 mmol) was added to a solution of 1,4-dimethoxybenzene (8.29 g, 60 mmol) and paraformaldehyde (3.00 g, 100 mmol) in 1,2-dichloroethane (250 mL), the mixture was stirred at room temperature for 40 min. Then, boron trifluoride diethyl etherate (6 mL, 47.6 mmol) was added to the solution and the mixture was stirred at 30 ℃ for 40 min. After the reaction was finished, the resulting oil was dissolved in CH_2Cl_2 (250 mL) and washed third with H_2O (300 mL). The organic layer was dried over anhydrous Na_2SO_4 and evaporated to afford the crude product. After purification by column chromatography using petroleum ether/ethyl acetate (V/V = 50:1) as the eluent, compound **2** as a white solid (1.67g, yield 35%) was isolated. Mp: 170-172 ℃. ^{1}H NMR ($CDCl_3$, 600 MHz), δ/ppm: 6.95-6.80 (m, 10H), 3.98-3.96 (t, J = 6.2 Hz, 2H), 3.80-3.70 (m, 37H), 2.93-2.61 (m, 2H), 1.83-1.71 (m, 4H), 1.34-1.31 (m, 2H), 1.25-0.68 (m, 10H). ^{13}C NMR ($CDCl_3$, 151 MHz), δ/ppm: 150.56, 150.40, 150.32, 150.22, 150.12, 149.54, 128.39, 128.23, 128.08, 127.90, 127.83, 114.60, 113.91, 113.27, 113.19, 113.08, 68.10, 55.69, 55.36, 55.26, 33.62, 31.56, 29.30, 29.27, 29.24, 29.15, 29.08, 27.59. ESI-MS m/z: calcd for $C_{54}H_{71}BrNO_{10}$ [**2** + NH_4]$^+$: 972.43; found: 972.43.

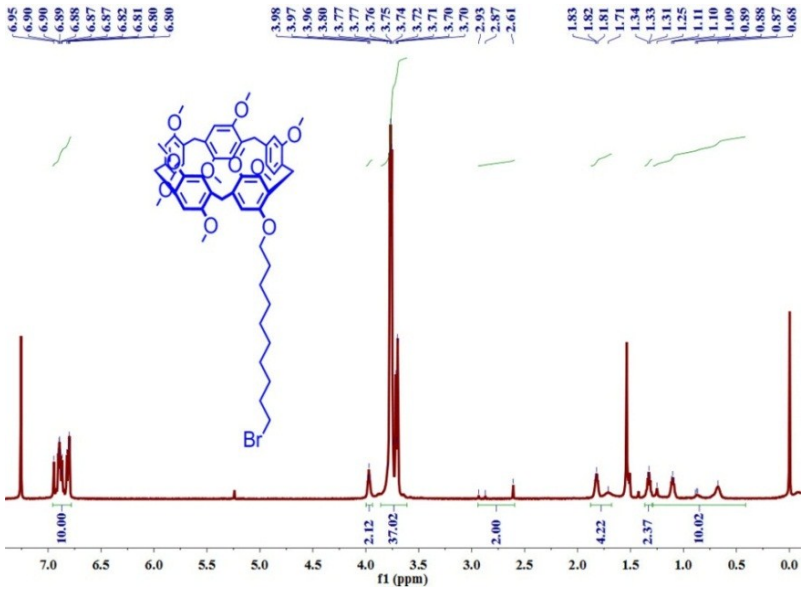

Fig. S4. ^{1}H NMR spectrum of compound **2** in $CDCl_3$.

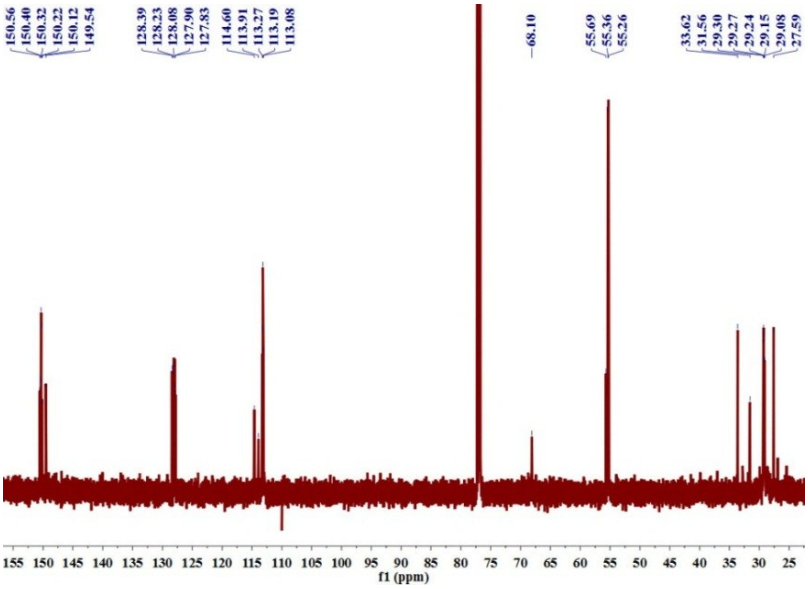

Fig. S5 ^{13}C NMR spectrum of compound **2** in $CDCl_3$.

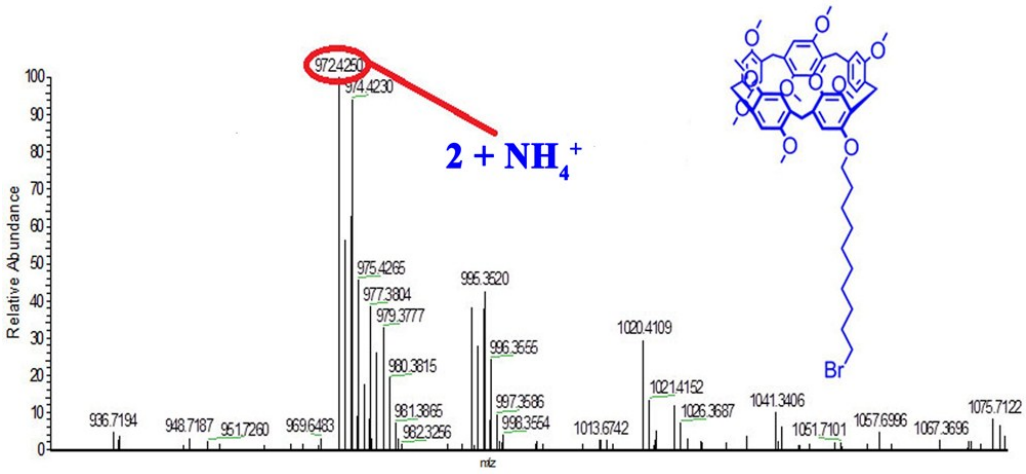

Fig. S6 ESI-MS spectrum of compound **2**.

Synthesis of compound 3. Compound **3** was synthesized by a similar route as Huang's.[S1] A mixture of bromo-functionalized copillar[5]arene (compound **2**) (0.95 g, 1.0 mmol) and phthalimide potassium (0.21 g, 1.1 mmol) in 30 mL of DMF was stirred at 90 ℃ for 24 h under nitrogen atmosphere. After adding water (100 mL), the resulting precipitates were collected by filtration and dried to give crude product. The crude product was dissolved in THF (30 mL), methanol (3 mL) and hydrazine hydrate (3 mL). After stirred at 50 ℃ for 24 h, the reaction mixture was concentrated by rotary evaporation. The resulting residue was dissolved in CH_2Cl_2 (150 mL) and washed with H_2O (2 × 200 mL). The organic layer was dried over anhydrous Na_2SO_4 and evaporated to afford the crude product, which was isolated by flash column chromatography using dichloromethane/methanol (V/V = 10 : 1). The fractions containing the product were combined and concentrated under vacuum to give compound 3 (0.70 g, yield 65%) as a white solid. Mp: 138-140 ℃. ^{1}H NMR (DMSO-d_6, 600 MHz), δ/ppm: 7.98-7.95 (m, 2H), 6.81-6.74 (m, 10H), 3.81-3.79 (t, J = 6.4Hz, 2H), 3.68-3.61 (m, 37H), 2.67-2.65 (t, J = 7.5Hz, 2H), 1.73-1.71 (m, 2H), 1.46-1.40 (m, 4H), 1.29-1.15 (m, 10H). ^{13}C NMR (DMSO-d_6, 151 MHz), δ/ppm: 150.42, 150.36, 150.31, 149.68, 127.94, 127.86, 127.83, 127.80, 127.78, 115.55,

114.40, 113.68, 113.61, 113.55, 68.12, 61.26, 55.78, 55.74, 55.70, 55.68, 55.62, 41.82, 33.13, 33.02, 29.33, 29.27, 26.42, 25.98, 25.87. ESI-MS m/z: calcd for $C_{54}H_{70}NO_{10}$ [**3** + H]$^+$: 892.50; found: 892.28.

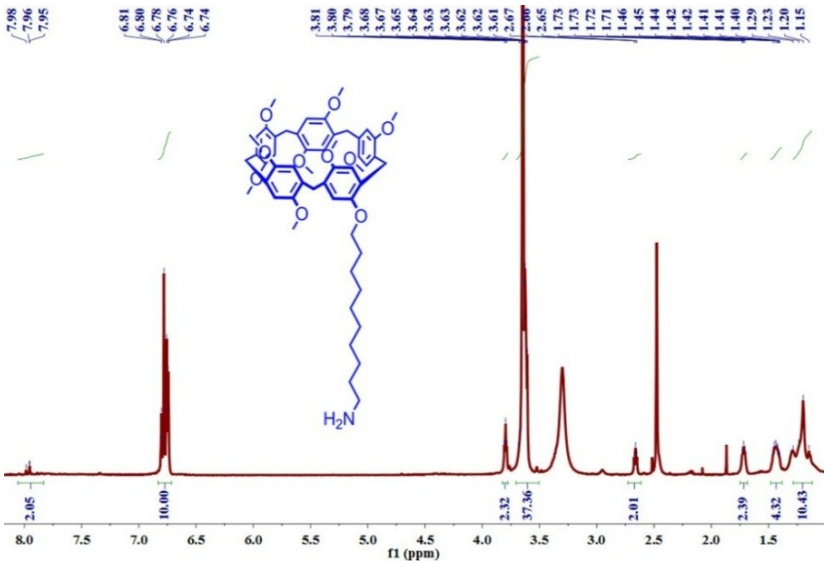

Fig. S7 ^{1}H NMR spectrum of compound **3** in DMSO-d_6.

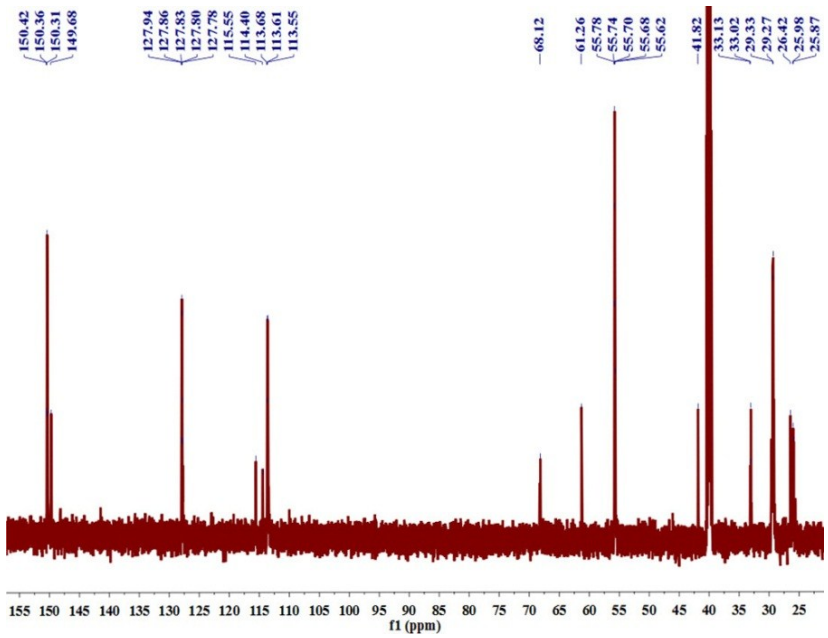

Fig. S8 ^{13}C NMR spectrum of compound **3** in DMSO-d_6.

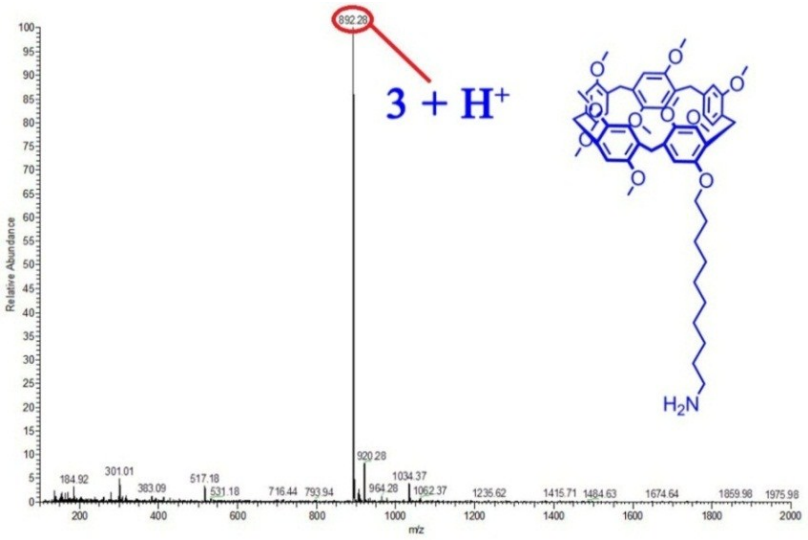

Fig. S9 ESI-MS spectrum of compound **3**.

Synthesis of compound P5N. Amino-functionalized copillar[5]arene (compound **3**) (1.2 mmol, 1.07 g) and 1,8-naphthalene anhydride (1.0 mmol, 0.20 g) were dissolved in 30 mL DMF and the reaction mixture was stirred at 140 ℃ for 30 h under a nitrogen atmosphere. Heating was stopped, the reaction mixture was cooled to room temperature and then poured into distilled water and filtered. The precipitate was dried under vacuum at 40 ℃ to obtain the crude product. It was purified by column chromatography using silica gel as stationary phase and petroleum ethers/ethyl acetate (V/V = 10 : 1) as eluent to get the desired product **P5N** as yellow solid (0.32 g, yield 30%). Mp: 70-72 ℃. ^{1}H NMR (DMSO-d_6, 400 MHz), δ/ppm: 8.53-8.45 (m, 4H), 7.94-7.85 (m, 2H), 6.79-6.73 (m, 10H), 4.06-3.81 (t, J = 7.6 Hz, 2H), 3.65-3.62 (m, 37H), 2.88-2.73 (m, 2H), 1.70-1.62 (m, 4H), 1.45-1.40 (m, 2H), 1.29-1.16 (m, 10H). ^{13}C NMR (DMSO-d_6, 151 MHz), δ/ppm: 164.17, 150.66, 150.53, 150.08, 134.44, 133.81, 131.58, 131.52, 131.13, 128.31, 128.14, 127.02, 126.90, 122.76, 114.79, 113.88, 68.50, 55.72, 55.70, 55.68, 55.64, 55.56, 40.48, 29.84, 29.55, 29.54, 29.52, 29.49, 29.41, 29.35, 29.27, 28.13, 27.14, 26.32. ESI-MS m/z: calcd for $C_{66}H_{74}NO_{12}$ [**P5N** + H]$^{+}$: 1072.52; found: 1072.52.

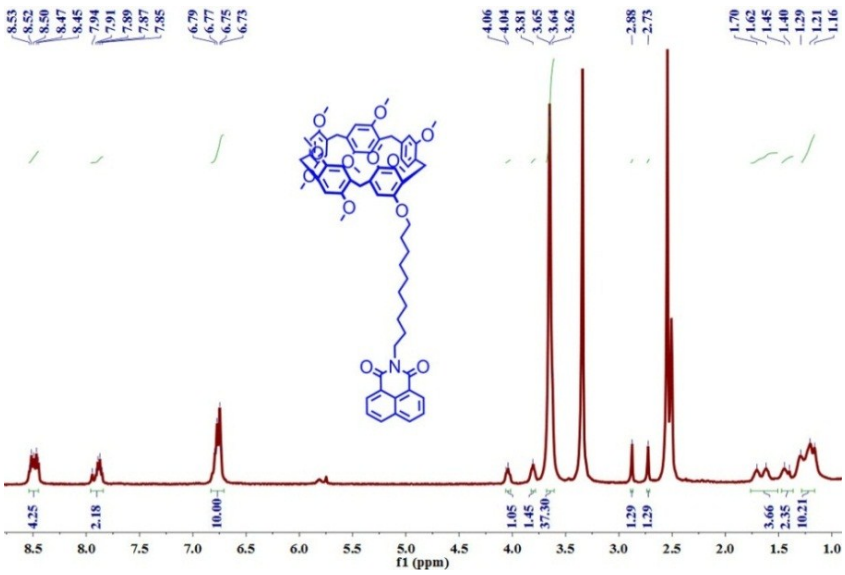

Fig. S10 ^{1}H NMR spectrum of **P5N** in DMSO-d_6.

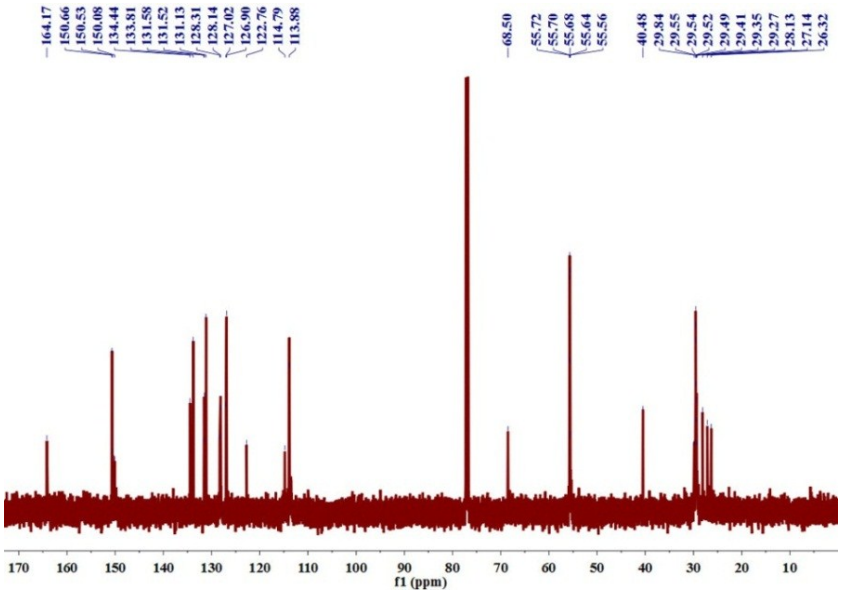

Fig. S11 ^{13}C NMR spectrum of **P5N** in $CDCl_3$.

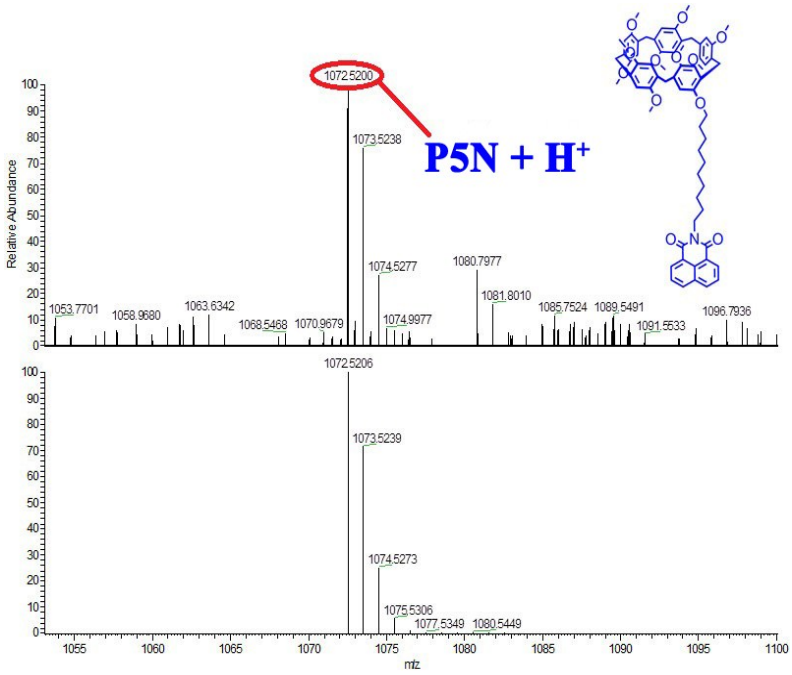

Fig. S12 ESI-MS spectrum of **P5N**.

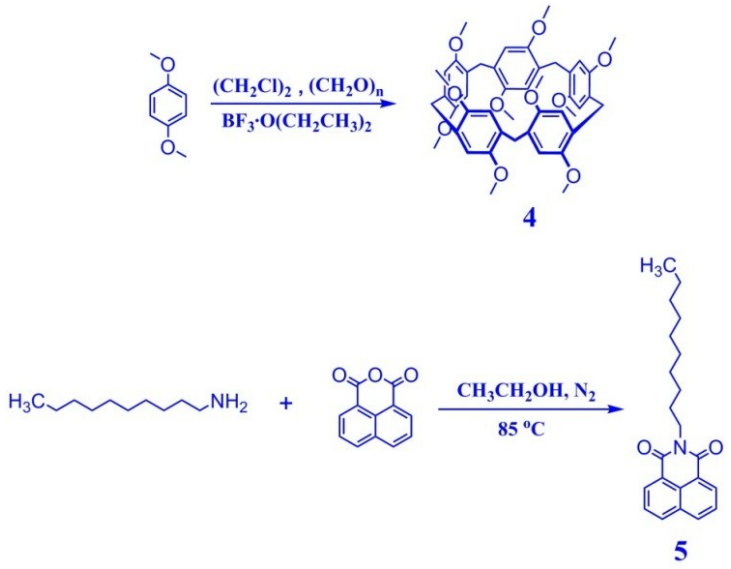

Scheme S2 Synthesis of compound [**4**-**5**].

Synthesis of compound 4. A mixture of 1,4-dimethoxybenzene (1.38 g, 10 mmol) and paraformaldehyde (0.90 g, 30 mmol) in 1,2-dichloroethane (100 mL) was stirred at room temperature for 30 min. Then, boron trifluoride diethyl etherate (5 mL, 23.8 mmol) was added to the solution and the mixture was stirred at 30 ℃ for 40 min. After the reaction was finished, the resulting oil was dissolved in CH_2Cl_2 (150 mL) and washed third with H_2O (300 mL). The organic layer was dried over anhydrous Na_2SO_4 and evaporated to afford the crude product. After purification by column chromatography using petroleum ether/ dichloromethane (V/V = 1:1) as the eluent, compound **4** as a white solid (0.60g, yield 40%) was isolated. Mp: 180-182 ℃. ^{1}H NMR ($CDCl_3$, 400 MHz), δ/ppm: 6.82 (s, 10H), 3.76 (s, 10H), 3.69 (s, 30H). ^{13}C NMR ($CDCl_3$, 101 MHz), δ/ppm: 150.63, 128.26, 113.85, 55.76, 29.52. ESI-MS m/z: calcd for $C_{45}H_{50}NaO_{10}$ [**4** + Na]$^+$: 773.33; found: 773.31.

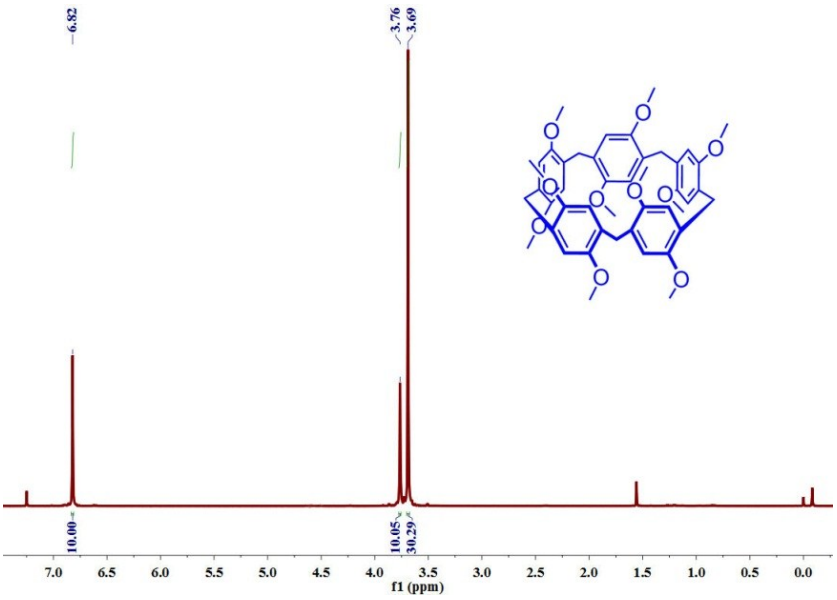

Fig. S13 ^{1}H NMR spectrum of compound **4** in $CDCl_3$.

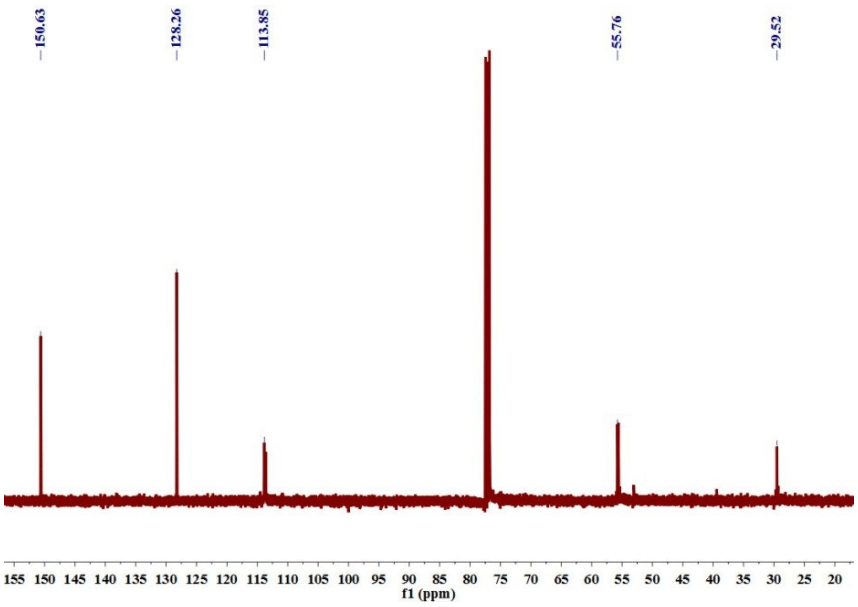

Fig. S14 ^{13}C NMR spectrum of compound **4** in $CDCl_3$.

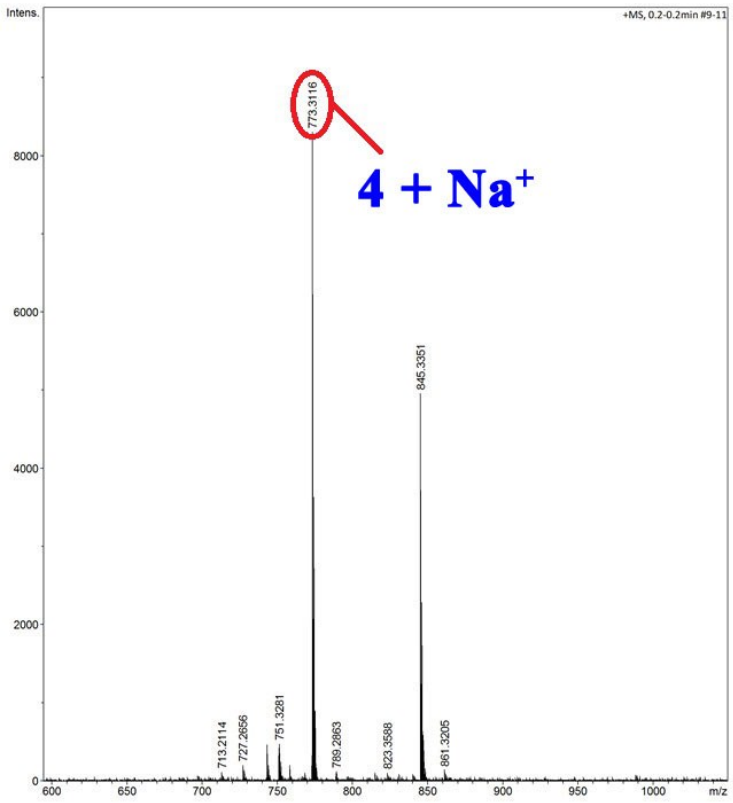

Fig. S15 ESI-MS spectrum of compound **4**.

Synthesis of compound 5. A mixture of 1-decylamine (0.39 g, 2.5 mmol) and 1,8-naphthalene anhydride (0.40 mmol, 2.0 mmol) in ethanol (60 mL) was stirred at 85 ℃ for 24h under nitrogen atmosphere. After reaction was finished, the solvent was cooled and filtered under reduced pressure. The crude product was elution with ethanol afforded compound **5** as a white solid (0.54 g, 80%). Mp: 77-78 ℃. ^{1}H NMR ($CDCl_3$, 400 MHz), δ/ppm: 8.57-8.54 (d, J = 9.4 Hz, 2H), 8.18-8.16 (d, J = 9.2 Hz, 2H), 7.73-7.69 (t, J = 7.5 Hz, 2H), 4.16-4.12 (t, J = 7.8 Hz, 2H), 1.74-1.69 (m, 2H), 1.42-1.23 (m, 14H), 0.85-0.82 (t, J = 4.6 Hz, 3H). ^{13}C NMR ($CDCl_3$, 101 MHz), δ/ppm: 164.25, 133.98, 133.78, 131.32, 131.11, 128.18, 126.97, 122.80, 40.59, 31.97, 29.66, 28.22, 27.25, 22.77, 14.21. ESI-MS m/z: calcd for $C_{22}H_{28}NO_2$ [**5** + H]$^+$: 338.21; found: 338.23.

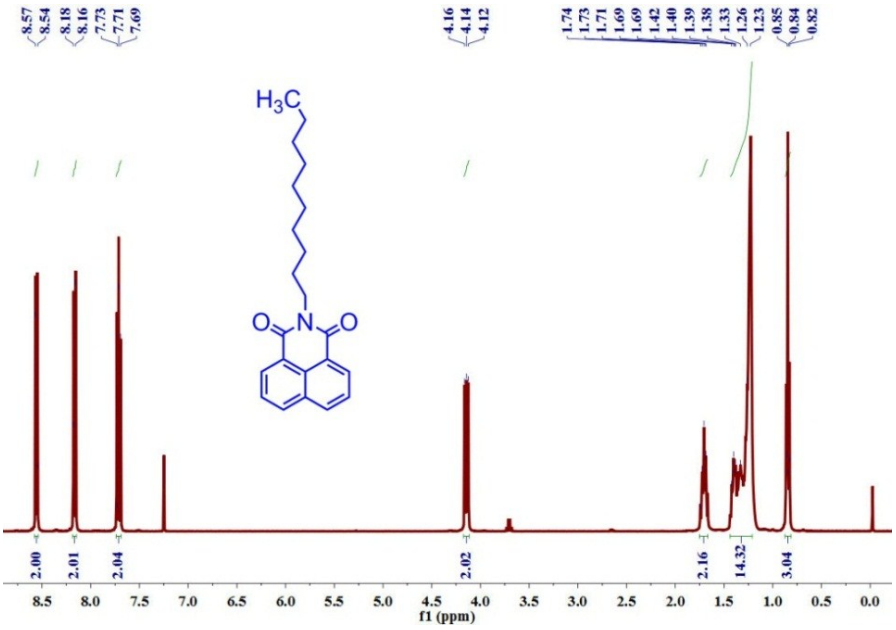

Fig. S16 ^{1}H NMR spectrum of compound **5** in $CDCl_3$.

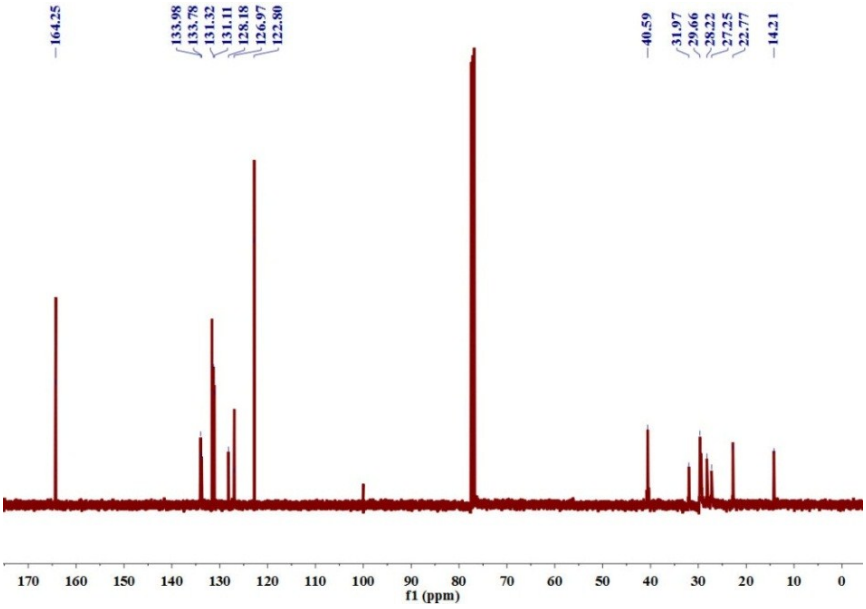

Fig. S17 ^{13}C NMR spectrum of compound **5** in $CDCl_3$.

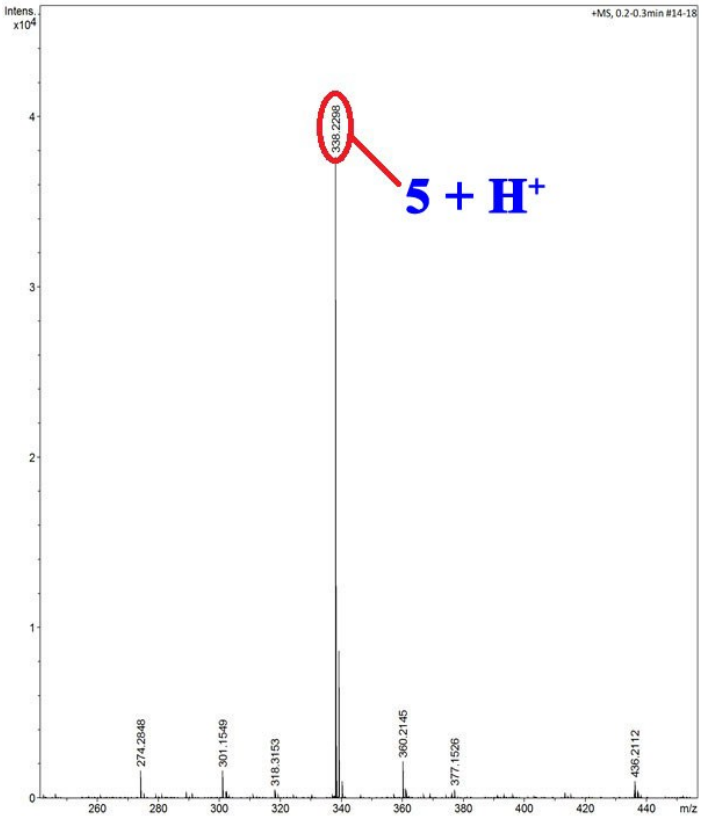

Fig. S18 ESI-MS spectrum of compound **5**.

Calculation method of emission quantum yield

Emission quantum yield was calculated by the following equation:

$$\emptyset = \emptyset_R \times \frac{I\,A_R}{I_R\,A}$$

Where Φ is emission quantum yield, I is the integrated emission intensity and A is the optical density (absorption). The subscript R refers to the reference of Quinine hemesulfate salt.

$$\emptyset = \emptyset_R \times \frac{I\,A_R}{I_R\,A} = 0.55 \times \frac{162.68}{153.02} \times \frac{0.0043}{0.0086} = 0.29$$

Table S1. Gelation Properties of Organogel **P5N-OG** in Organic Solvents

Entry	Solvent	State[a]	CGC[b](%)	T_{gel}[c](℃,wt%)
1	water	P	\	\
2	acetone	P	\	\
3	methanol	P	\	\
4	ethanol	P	\	\
5	isopropanol	P	\	\
6	isopentanol	P	\	\
7	acetonitrile	P	\	\
8	THF	S	\	\
9	DMF	S	\	\
10	DMSO	S	\	\
11	CCl_4	S	\	\
12	n-hexane	P	\	\
13	ethanediol	P	\	\
14	tert-butylalcohol	P	\	\
15	CH_2Cl_2	S	\	\
16	$CHCl_3$	S	\	\
17	CH_2ClCH_2Cl	S	\	\
18	petroleum ether	P	\	\
19	ethyl acetate	P	\	\
20	n-propanol	P	\	\
21	n-butyl alcohol	P	\	\
22	cyclohexanol	G	5	50 ~ 52℃(5%)
23	n-hexanol	P	\	\
24	propanetriol	P	\	\

[a]G, P and S denote gelation, precipitation and solution, respectively;
[b]The critical gelation concentration (wt%, 10 mg/ml = 1.0 %);

[c]The gelation temperature (℃).

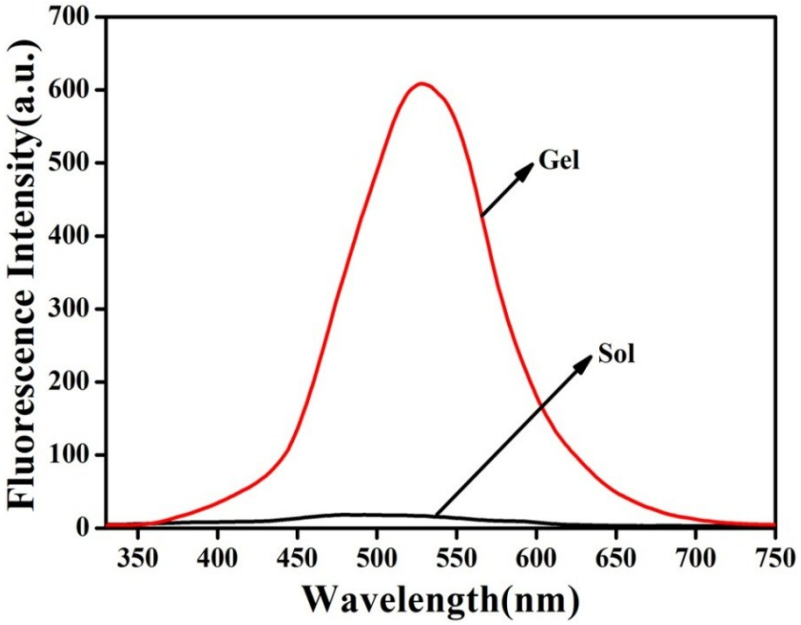

Fig. S19 Temperature-dependent fluorescence spectra of **P5N-OG** (in cyclohexanol, 5% (w/v)) during gelation process (λ_{ex} = 297 nm).

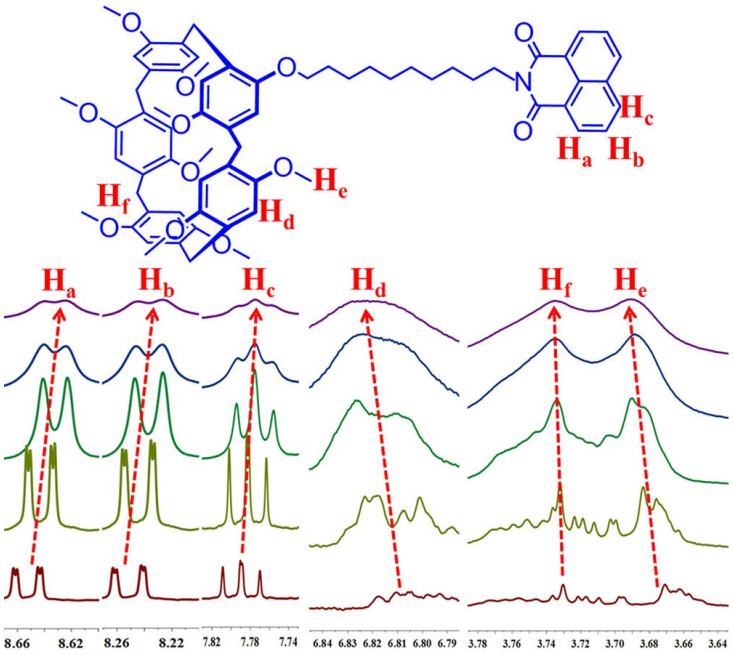

Fig. S20 Partial concentrations-dependent ^{1}HNMR spectra of **P5N** in $CDCl_3$, from bottom to top: 3.7 × 10^{-3} M, 9.3 × 10^{-3} M, 1.9 × 10^{-2} M, 2.8 × 10^{-2} M, 3.7 × 10^{-2} M.

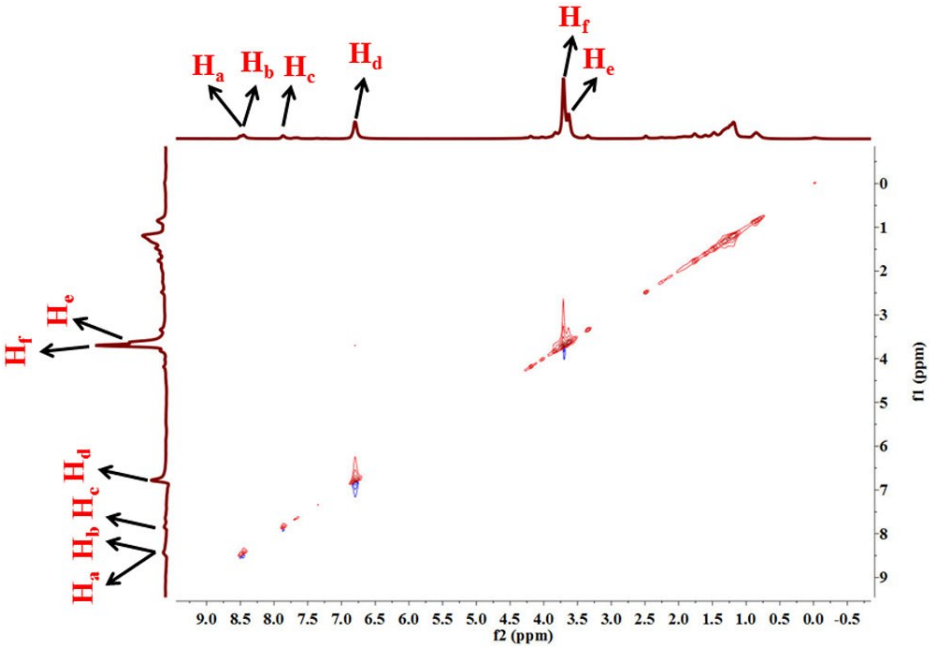

Fig. S21 2D NOESY NMR spectrum of **P5N** (30 mM) in DMSO-d_6 solution.

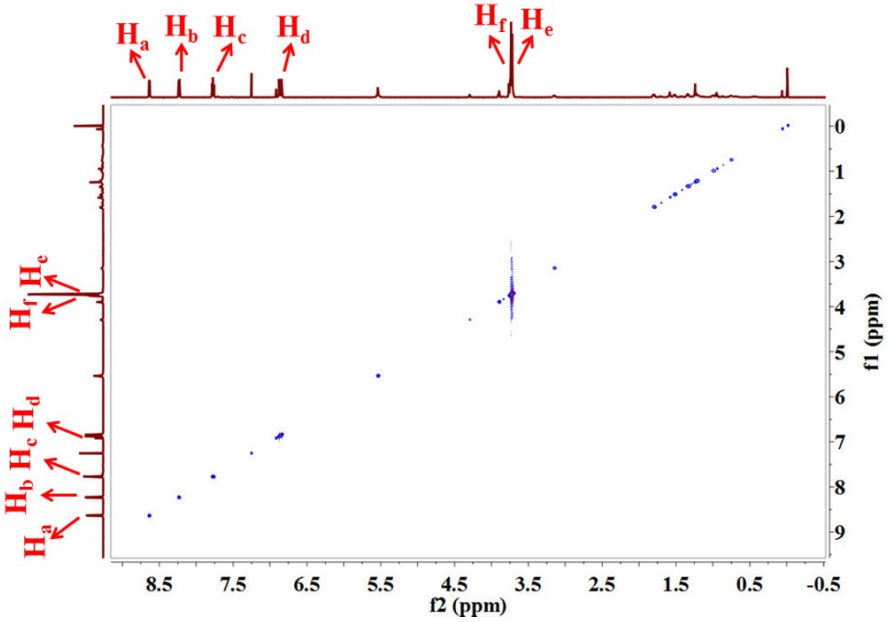

Fig. S22 2D NOESY NMR spectrum of **P5N** (30 mM) in $CDCl_3$ solution.

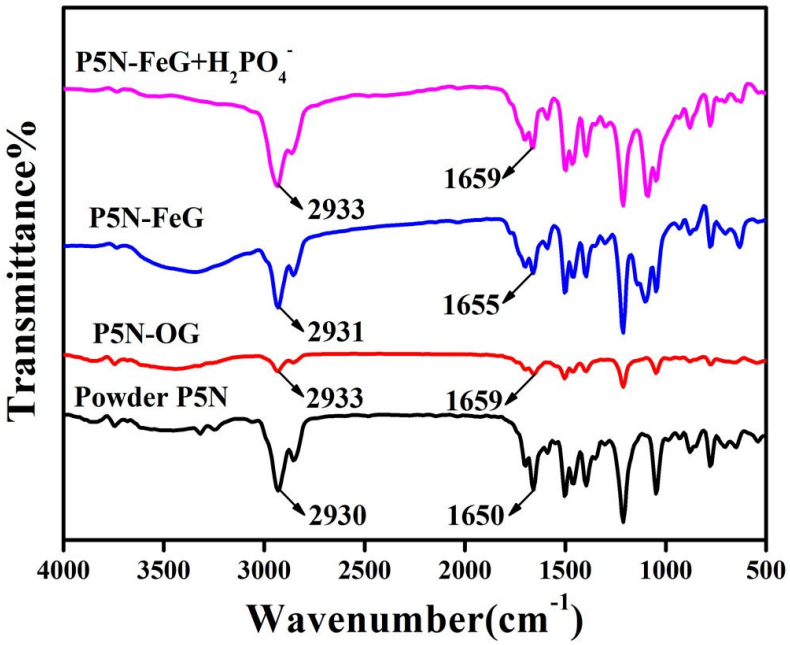

Fig. S23 FT-IR spectra of powdered **P5N**, xerogel **P5N-OG**, xerogel **P5N-FeG**, and xerogel **P5N-FeG** + $H_2PO_4^-$

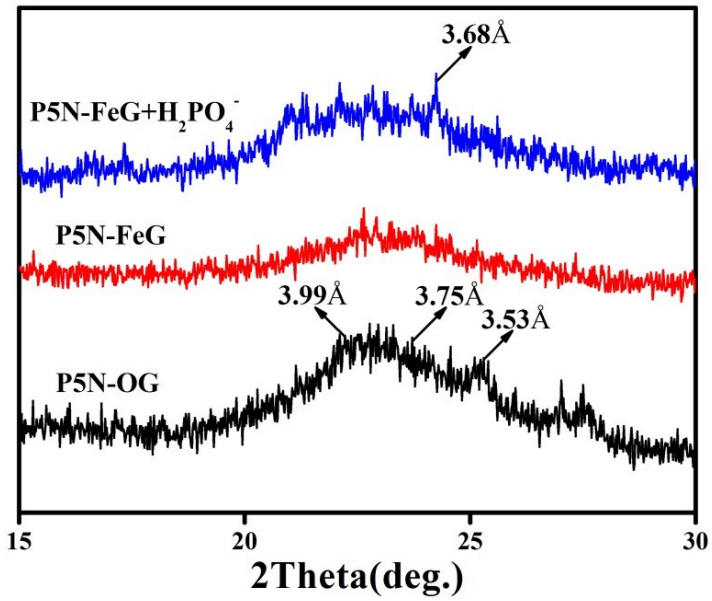

Fig. S24 Powder XRD patterns of xerogel **P5N-OG**, xerogel **P5N-FeG**, and xerogel **P5N-FeG** + $H_2PO_4^-$.

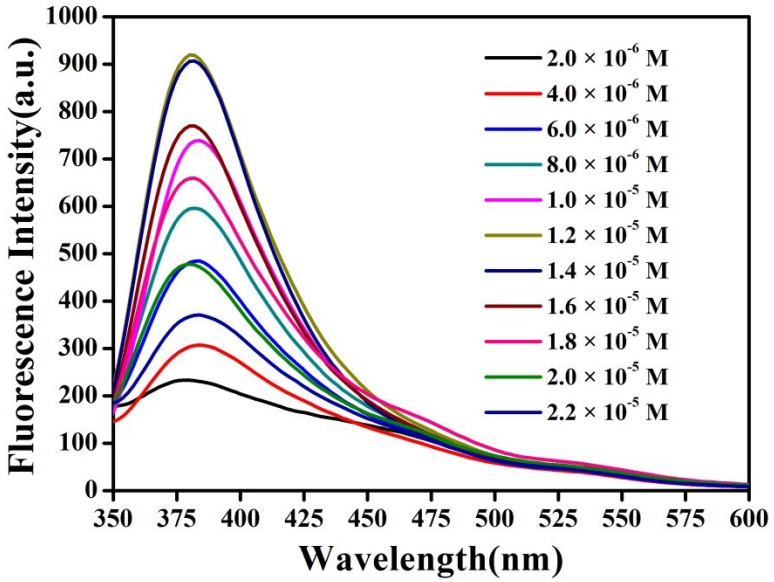

Fig. S25 Fluorescence spectra of permethyl-pillar[5]arene (compound **4**) in the presence of different concentration of naphthalimide monomer (compound **5**) in cyclohexanol at room temperature (λ_{ex} = 265 nm).

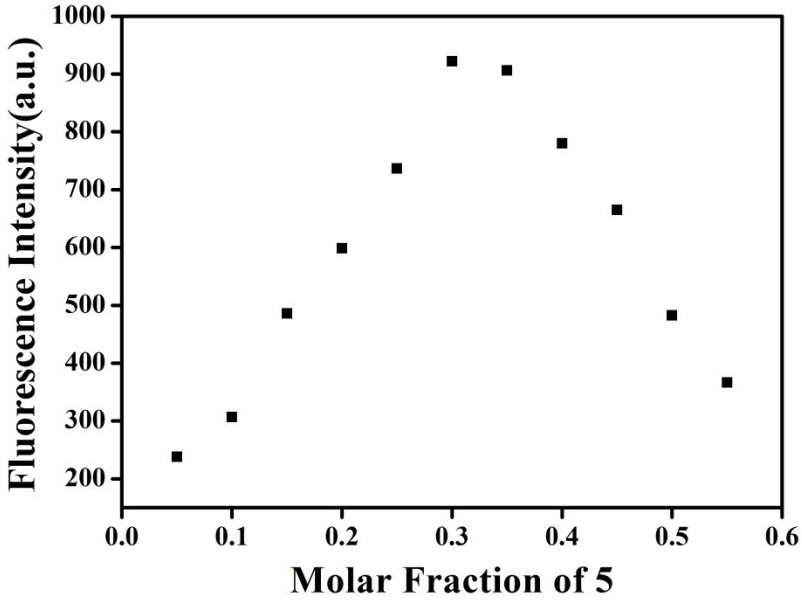

Fig. S26 Job's plot showing the 2:1 stoichiometry of the complexation between permethyl-pillar[5]arene (model compound **4**) (2×10^{-4} M) and naphthalimide monomer (model compound **5**) (0.1 M) in cyclohexanol by plotting the fluorescence intensity at λ_{ex} = 265 nm.

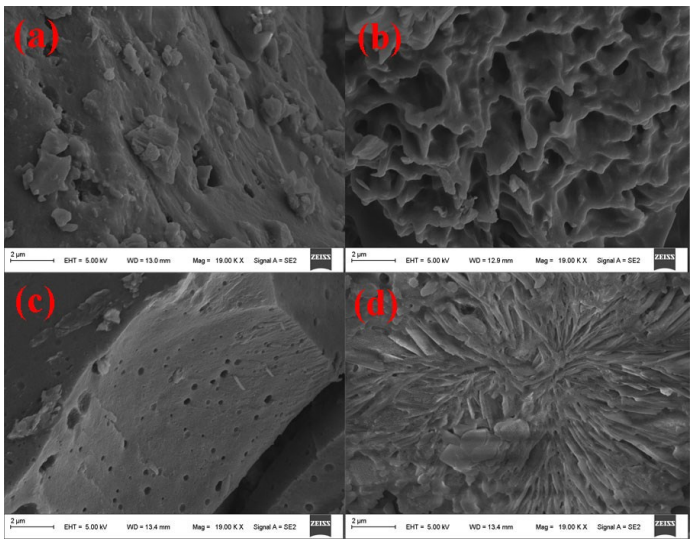

Fig. S27 SEM images of (a) powder **P5N**; (b) xerogel **P5N-OG**; (c) xerogel **P5N-FeG**; (c) xerogel **P5N-FeG** + $H_2PO_4^-$.

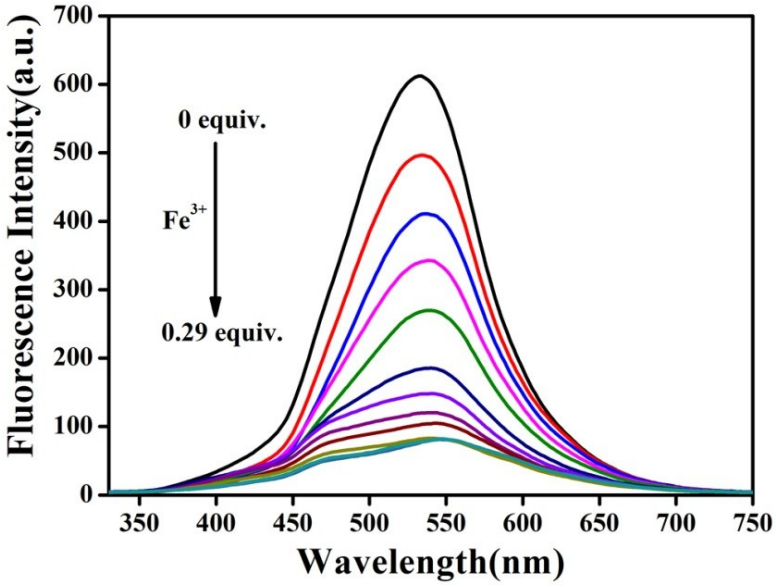

Fig. S28 Fluorescence spectra of **P5N-OG** (in cyclohexanol, 5% (w/v)) with increasing concentration of Fe^{3+} (λ_{ex} = 297 nm).

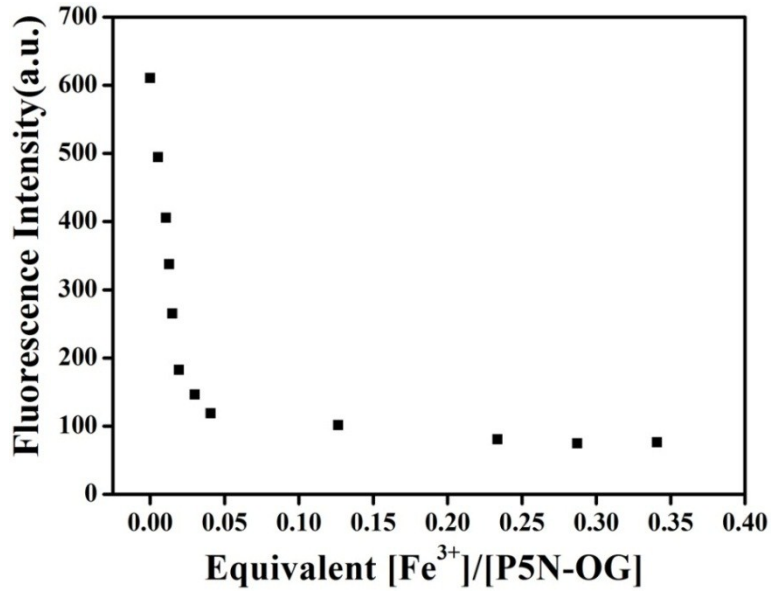

Fig. S29 A plot of emission at 530 nm versus number of equivalents of Fe^{3+}.

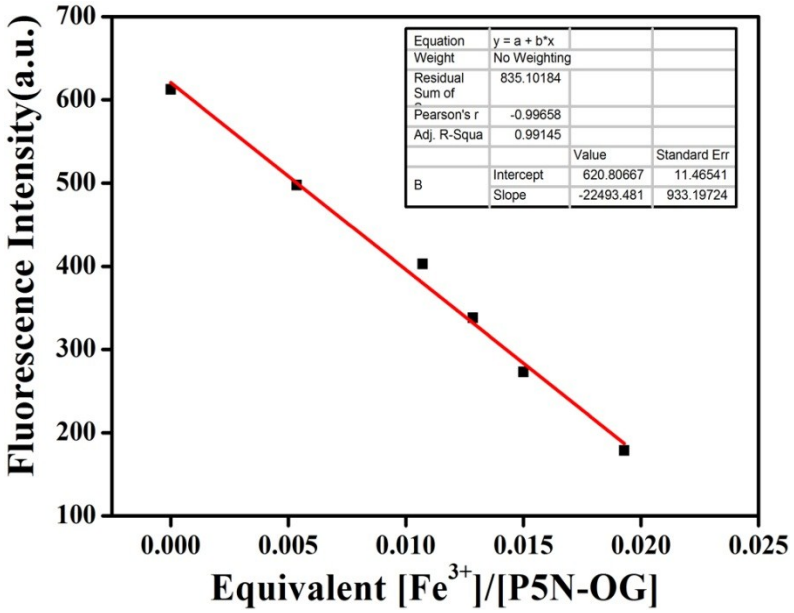

Fig. S30 The photograph of the linear range for Fe^{3+}.

The result of the analysis as follows:

Linear Equation: $Y = -22493.48 \times X + 620.81$ $R^2 = 0.99145$

$S = 2.2493 \times 10^{10}$

$$\delta = \sqrt{\frac{\sum_{i=1}^{N}(F_i - \bar{F})}{N-1}} = 1.08 \qquad (N = 20) \qquad K = 3$$

$$LOD = K \times \delta / S = 0.145\ nM$$

Table S2. Comparison of the Analytical Performance of the Fluorescence Sensing Systems for Fe^{3+}

Fluorescent materials	Limit of Detection	Refs
carbon nanodots	40 nM	S2
MIL-53(Al)	900 nM	S3
Rhodamine-Functionalized Graphene Quantum Dots	20 nM	S4
Sulfur-doped graphene quantum dots (S-GQDs)	4.2 nM	S5
Nap-Glc	42.7 nM	S6
furfuran-based rhodamine B fluorescent chemosensor	25 nM	S7
color-tunable N-doped carbon dots (NCDs)	520 nM	S8
carbon nanodots-based nanoprobe	10 nM	S9
TPA-BODIPY-OH	515 nM	S10
supramolecular organogel (**P5N-OG**)	0.145 nM	This work

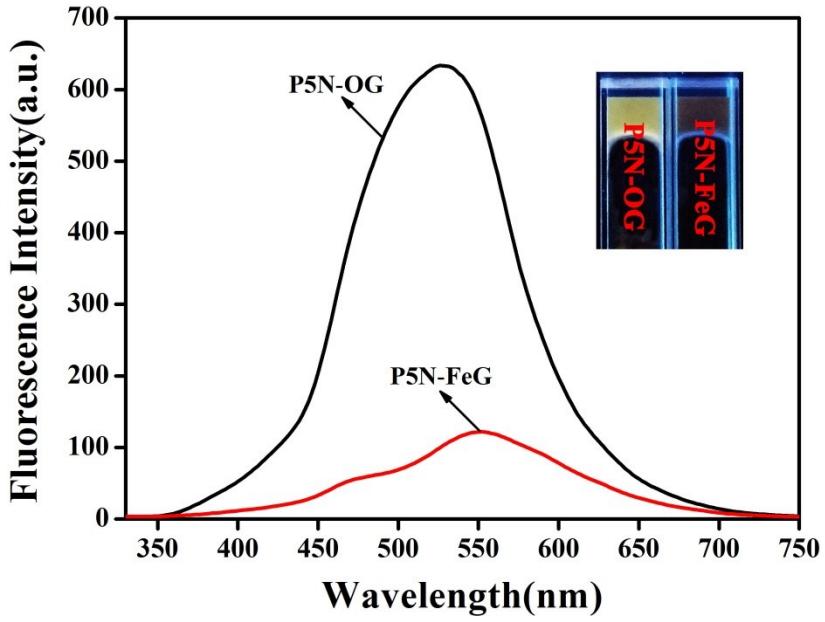

Fig. S31 Fluorescence spectra of **P5N-OG** (in cyclohexanol, 5% (w/v)) in the presence of solid samples of iron (III) perchlorate hexahydrate (0.00094 g, 0.29 equiv.) at room temperature (λ_{ex} = 297 nm).

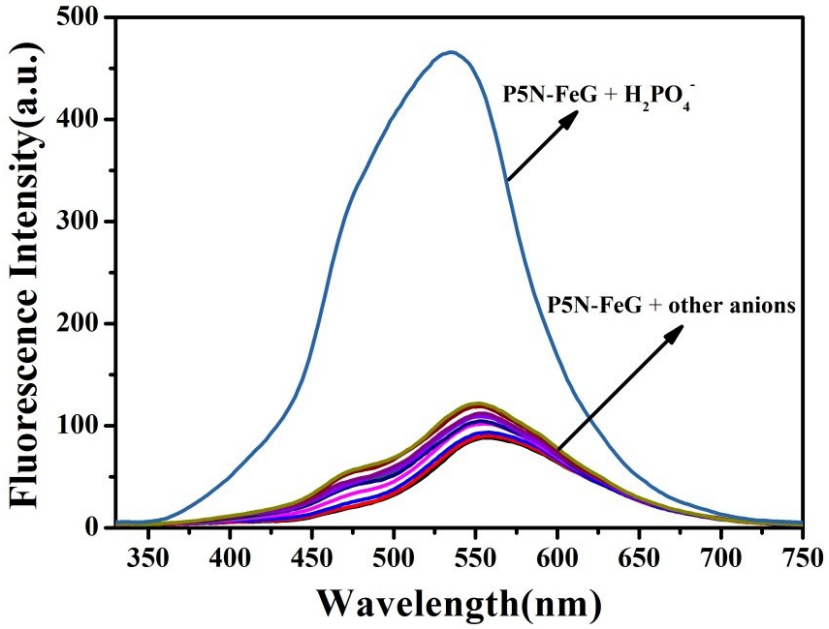

Fig. S32 Fluorescence spectra of **P5N-OG** (in cyclohexanol, 5% (w/v)) in the presence of various anions (F^-, Cl^-, Br^-, I^-, AcO^-, $H_2PO_4^-$, HSO_4^-, ClO_4^-, SCN^-, and CN^-) at room temperature (λ_{ex} = 297 nm).

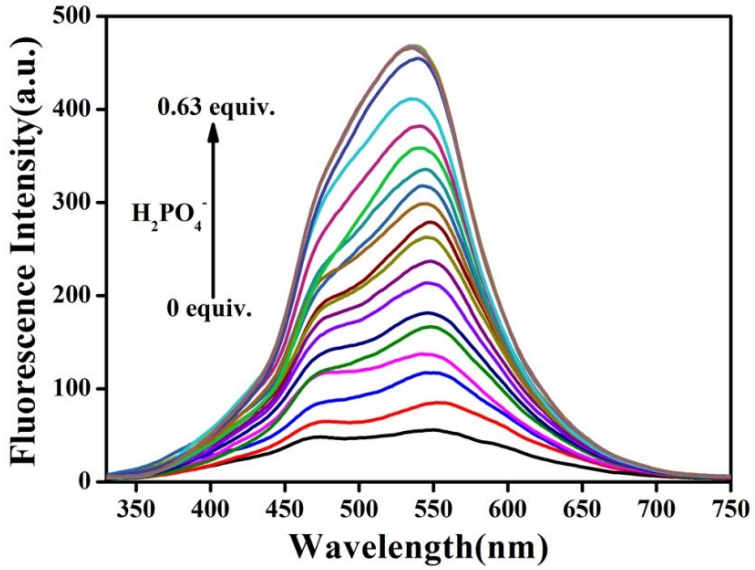

Fig. S33 Fluorescence spectra of **P5N-FeG** (in cyclohexanol, 5% (w/v)) with increasing concentration of $H_2PO_4^-$ (λ_{ex} = 297 nm).

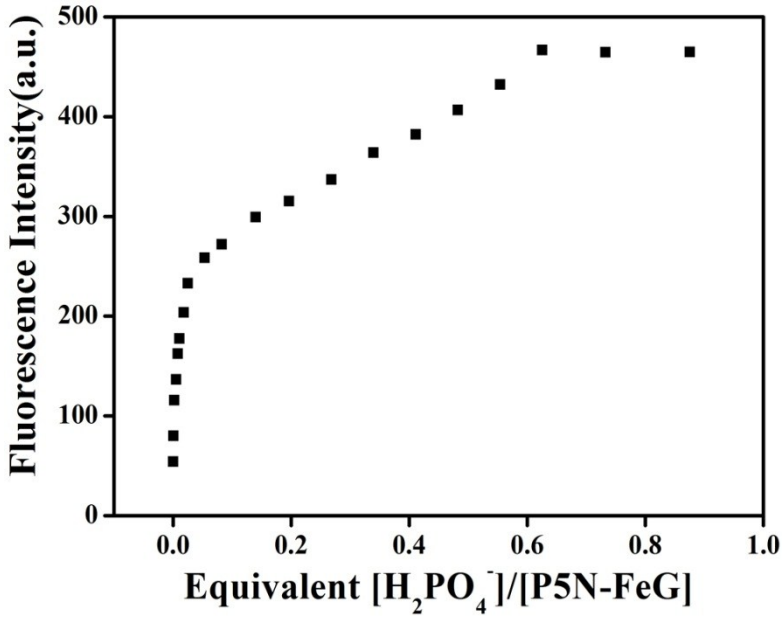

Fig. S34 A plot of emission at 530 nm versus number of equivalents of $H_2PO_4^-$.

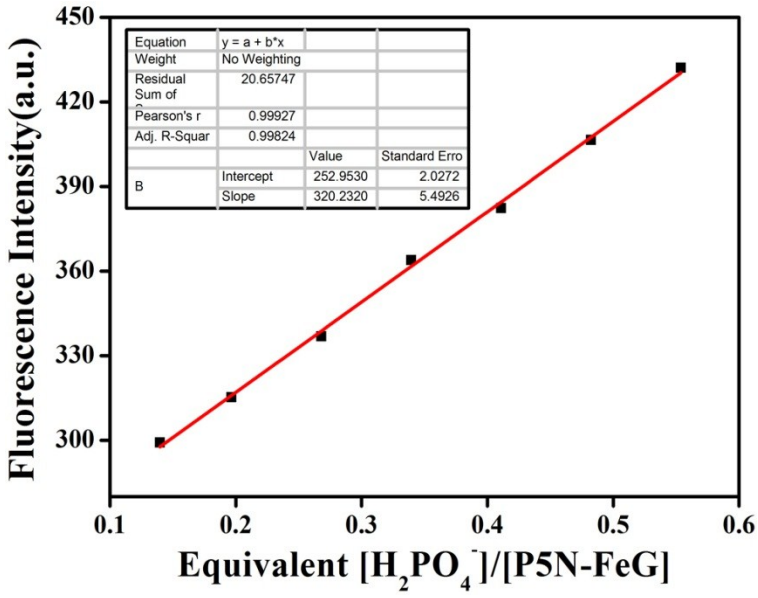

Fig. S35 The photograph of the linear range for $H_2PO_4^-$.

The result of the analysis as follows:

Linear Equation: Y = 320.23 × X + 252.95 R^2 = 0.99824

S = 3.20×10^8

$$\delta = \sqrt{\frac{\sum_{i=1}^{N}(F_i - \bar{F})}{N-1}} = 1.10 \quad (N = 20) \quad K = 3$$

LOD = K × δ/S = 10.3 nM

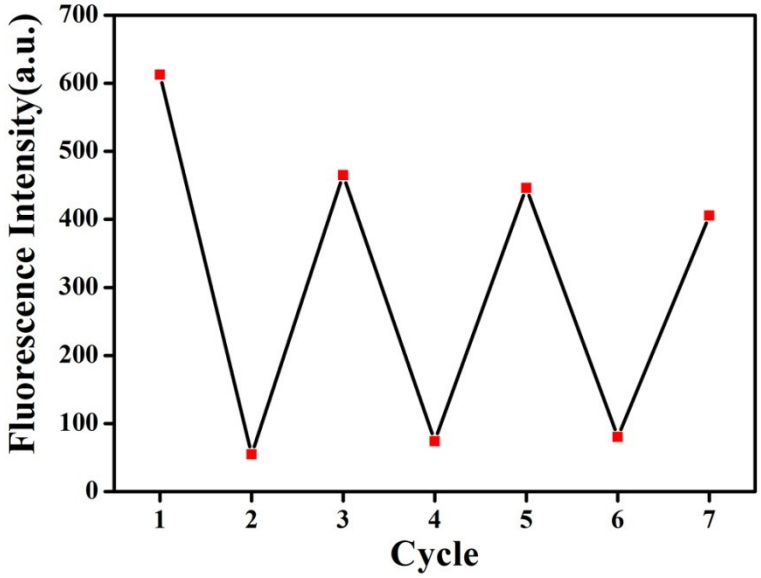

Fig. S36 Fluorescent "on-off-on" cycles of **P5N-OG**, controlled by the alternative addition of Fe^{3+} and $H_2PO_4^-$ (λ_{ex} = 297 nm).

Table S3. The ICP Date of **P5N-OG** with Fe^{3+}

Ion	Initial concentration (M)	Residual concentration (M)	Absorbing rate %
Fe^{3+}	1.0×10^{-4}	5.78×10^{-7}	99.42%

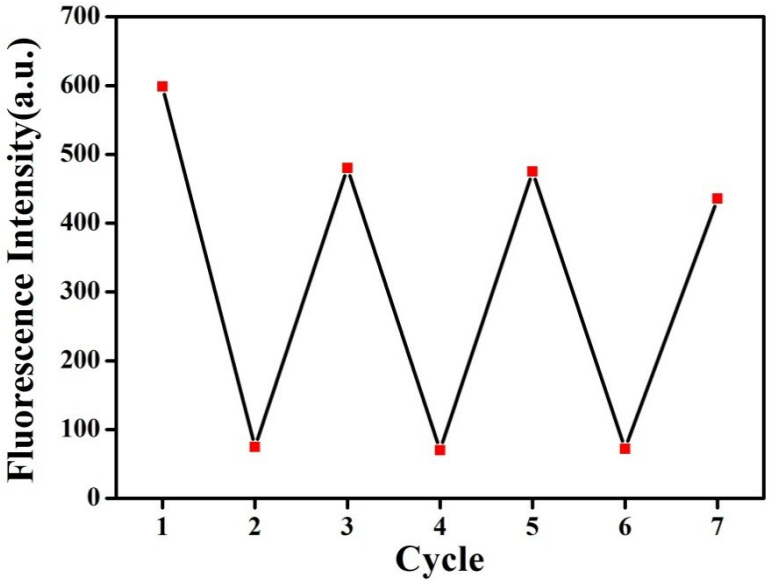

Fig. S37 Recyclable separation of Fe^{3+} (λ_{ex} = 297 nm).

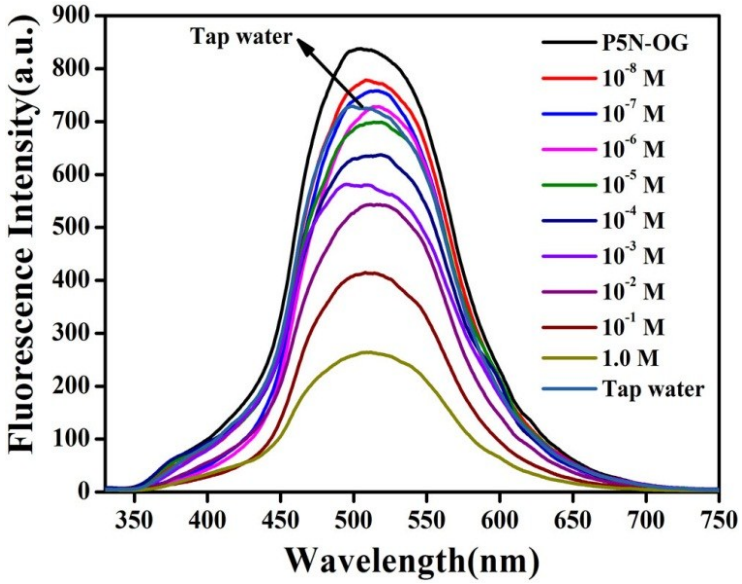

Fig. S38 Fluorescence spectra of **P5N-OG** (in cyclohexanol, 5% (w/v)) in different concentration of Fe^{3+} at room temperature (λ_{ex} = 297 nm).

Table S4. The ICP Date of Tap Water with Fe^{3+}

Analyte	Ion	Concentration (M)
Tap water	Fe^{3+}	1.1×10^{-6}

Reference

(S1) Z. Zhang, C. Han, G. Yu and F. Huang, *Chem. Sci.*, 2012, **3**, 3026.

(S2) P. Miao, Y. Tang, K. Han and B. Wang, *J. Mater. Chem. A*, 2015, **3**, 15068.

(S3) C.-X. Yang, H.-B. Ren and X.-P. Yan, *Anal. Chem*., 2013, **85**, 7441.

(S4) R. Guo, S. Zhou, Y. Li, X. Li, L. Fan and N. H. Voelcker, *ACS Appl. Mater. Interfaces*, 2015, **7**, 23958.

(S5) S. Li, Y. Li, J. Cao, J. Zhu, L. Fan and X. Li, *Anal. Chem*., 2014, **86**, 10201.

(S6) F. Liu, P. Tang, R. Ding, L. Liao, L. Wang, M. Wang and J. Wang, *Dalton Trans.*, 2017, **46**, 7515.

(S7) T. Zhou, X. Chen, Q. Hua, W. Lei, Q. Hao, B. Zhou, C. Su, X. Bao, *Sens. Actuators B*, 2017, **253**, 292.

(S8) Y. Song, C. Zhu, J. Song, H. Li, D. Du and Y. Lin, *ACS Appl. Mater. Interfaces*, 2017, **9**, 7399.

(S9) C. Wang, Y. Huang, K. Jiang, M. G. Humphrey and C. Zhang, *Analyst*, 2016, **141**, 4488.

(S10) B. Shen and Y. Qian, *J. Mater. Chem. B*, 2016, **4**, 7549.